Ndel1-derived peptides modulate bidirectional transport of injected beads in the squid giant axon

Michal Segal[1], Ilya Soifer[1], Heike Petzold[2], Jonathon Howard[2], Michael Elbaum[3] and Orly Reiner[1,*]

[1]Department of Molecular Genetics, The Weizmann Institute of Science, Rehovot 76100, Israel
[2]Max Planck Institute of Molecular Cell Biology and Genetics, 01307 Dresden, Germany
[3]Department of Materials and Interfaces, The Weizmann Institute of Science, Rehovot 76100, Israel
*Author for correspondence (orly.reiner@weizmann.ac.il)

Biology Open 1, 220–231
doi: 10.1242/bio.2012307

Summary

Bidirectional transport is a key issue in cellular biology. It requires coordination between microtubule-associated molecular motors that work in opposing directions. The major retrograde and anterograde motors involved in bidirectional transport are cytoplasmic dynein and conventional kinesin, respectively. It is clear that failures in molecular motor activity bear severe consequences, especially in the nervous system. Neuronal migration may be impaired during brain development, and impaired molecular motor activity in the adult is one of the hallmarks of neurodegenerative diseases leading to neuronal cell death. The mechanisms that regulate or coordinate kinesin and dynein activity to generate bidirectional transport of the same cargo are of utmost importance. We examined how Ndel1, a cytoplasmic dynein binding protein, may regulate non-vesicular bidirectional transport. Soluble Ndel1 protein, Ndel1-derived peptides or control proteins were mixed with fluorescent beads, injected into the squid giant axon, and the bead movements were recorded using time-lapse microscopy. Automated tracking allowed for extraction and unbiased analysis of a large data set. Beads moved in both directions with a clear bias to the anterograde direction. Velocities were distributed over a broad range and were typically slower than those associated with fast vesicle transport. Ironically, the main effect of Ndel1 and its derived peptides was an enhancement of anterograde motion. We propose that they may function primarily by inhibition of dynein-dependent resistance, which suggests that both dynein and kinesin motors may remain engaged with microtubules during bidirectional transport.

Key words: Microtubules, Cytoplasmic dynein, Kinesin, Retrograde transport, Anterograde transport

Introduction

Long-distance intracellular transport is typically conducted by microtubule-associated molecular motors. Most members of the kinesin superfamily move toward the plus ends of microtubules, while the dynein complex is the main motor moving toward the minus ends of microtubules. Numerous vesicular and molecular cargoes are attached to these motors. Neurons, and in particular axons, which contain long, unipolar parallel microtubule arrays primarily orienting with the plus end towards the synapse, are very sensitive to impaired motor activity. Aberrant intracellular transport has been suggested as a common underlying theme for multiple neurodegenerative diseases such as Alzheimer's disease, ALS (amyotrophic lateral sclerosis), Parkinson disease and Huntington disease (Chevalier-Larsen and Holzbaur, 2006; Colin et al., 2008; Dompierre et al., 2007; Duncan and Goldstein, 2006; Holzbaur, 2004; Levy and Holzbaur, 2006; Perlson et al., 2009; Stokin and Goldstein, 2006). One of the major challenges is to characterize normal transport. However, this task is not simple. There is a growing realization that many cargoes bind multiple motors in vivo and show complex transport patterns involving movements in both anterograde and retrograde directions (Ally et al., 2009; Encalada et al., 2011; Guerin et al., 2010; Holzbaur and Goldman, 2010; Ma and Chisholm, 2002; Rogers et al., 1997; Scott et al., 2011; Shubeita et al., 2008).

Our understanding of the way in which bidirectional transport is successfully achieved in vivo is still rudimentary, although several models and experimental designs have been tested (Gross, 2004; Muller et al., 2008; Muller et al., 2010). How transport directionality is regulated temporally is even less understood. One direction looks to biochemical regulation, perhaps involving factors that affect the activities of kinesin and dynein motors, such as tau (Dixit et al., 2008; Mandelkow et al., 2004; Vershinin et al., 2007; Vershinin et al., 2008). Another direction suggests mechanical competition between sets of anterograde and retrograde directed motors (Guerin et al., 2010; Muller et al., 2008). One molecular complex that regulates different motors is dynactin; it contributes to dynein-based motility (Schroer, 2004; Vallee et al., 2004) but also regulates kinesins 2 and 5 (Berezuk and Schroer, 2007; Deacon et al., 2003; Gross, 2003; Haghnia et al., 2007; Martin et al., 1999). The LIS1-containing complex is also known to regulate dynein activity. LIS1 and its interacting partners Nde1 and Ndel1 directly affect the activity of cytoplasmic dynein (McKenney et al., 2010; Mesngon et al., 2006; Shmueli et al., 2010; Yamada et al., 2008). Nde1 interacts with LIS1, several centrosomal proteins, and dynein light and intermediate chains (Feng et al., 2000; Feng and Walsh, 2004; Hirohashi et al., 2006a; Hirohashi et al., 2006b; Stehman et al., 2007). Ndel1 is found in complex

with LIS1, and with dynein heavy and intermediate chains (Niethammer et al., 2000; Sasaki et al., 2000). Thus, it is possible that Ndel1 is one of the biochemical factors that influence competition between forces generated by distinct molecular motor types.

We have tested the role of mammalian Ndel1 and specific peptides derived from it in the squid giant axon, which is an excellent model system in which to study neuronal transport (Allen et al., 1982; Bearer et al., 2000; Terada et al., 2000; Terasaki et al., 1995; Vale et al., 1985b). The axon contains plumes of organized microtubules (Bearer and Reese, 1999) and expresses members of both the kinesin superfamily (DeGiorgis et al., 2008; Vale et al., 1985a) and cytoplasmic dynein (Schnapp and Reese, 1989) molecular motors. Squid axoplasm has been used for in vitro assays (Brady et al., 1982; Brady et al., 1985; DeGiorgis et al., 2008; Kuznetsov et al., 1992; Vale et al., 1985a; Vale et al., 1985c), while the intact squid axon has been used as an in vivo system to follow transport of fluorescent proteins or negatively charged beads (Bearer et al., 2000; Terada et al., 2000; Terasaki et al., 1995). The motility of the population of negatively charged beads within injected axons has been shown to fit slow motility (Terada et al., 2000; Terasaki et al., 1995). A recent study has demonstrated that many cytosolic proteins travel in mammalian axons using a similar slow motor dependent transport (Scott et al., 2011). We injected negatively charged fluorescent beads into the squid giant axon together with mammalian Ndel1, Ndel1-derived peptides, or control proteins, and monitored their transport using time-lapse confocal microscopy as previous described (Bearer et al., 2000; Satpute-Krishnan et al., 2003; Satpute-Krishnan et al., 2006). Our analysis involved the use of automated tracking combined with large-scale, unbiased statistical analysis. The results confirm slow but processive motility of negatively charged beads and reveal distinct effects of the individual peptides on bead movements.

Results

Ndel1 structure prediction and peptide selection

Short folded peptides derived from a protein are likely to reveal functional activities, which may be masked in full-length proteins due to changes in conformation. We chose our peptides based on their structure within the full-length protein. The target of our study, the Ndel1 protein was predicted to be unstructured using the FoldIndex prediction algorithm (http://bip.weizmann.ac.il/fldbin/findex) (Prilusky et al., 2005), with the exception of approximately fifty amino acids surrounding amino acid 250 (Fig. 1A). This domain is predicted to form a beta-sheet (http://www.ics.uci.edu/~baldig/betasheet.html). In addition, it contains the cysteine (C273) that can undergo lipid modification (Shmueli et al., 2010). We have demonstrated that palmitoylation of C273 negatively regulates the interaction between Ndel1 and cytoplasmic dynein (Shmueli et al., 2010). Other programs such as COILS (http://www.ch.embnet.org/software/COILS_form.html), and more importantly direct structural data for residues 6–166, indicate that the N-terminal part of Ndel1 forms a coiled-coil structure divided into three regions (Fig. 1B) (Derewenda et al., 2007). The dimerization domain of Ndel1 is composed of residues 8–99 (Derewenda et al., 2007). Residues 103–153 contain the minimal LIS1-binding domain within the N-terminal part of Ndell; deletion of twenty amino acids (114–133) was sufficient to abrogate the interaction with LIS1 (Yan et al., 2003). In this study we were interested in investigating LIS1-independent activities of Ndel1. Therefore, based on the above information we generated two peptides from Ndel1: DID, consisting of amino acids 4–103 and pep3, consisting of amino acids 238–284 (schematically shown in Fig. 1C). Based on the limited amino acid similarity between Nde1 and Ndel1 within the DID domain (supplementary material Fig. S1), we also generated one corresponding peptide from Nde1 DID amino acids 3–102 (Nde1-DID). All peptides were fused to gluthathione S-transferase (GST) for easy purification and solubility. GST was used as a control peptide in all experiments.

Protein interactions of these peptides were examined by pull-down experiments (Fig. 1D–E). Our results indicate that Ndel1 and the three peptides pulled down a relatively small amount of conventional kinesin in brain extract, nonetheless no interaction was observed with the control GST peptide (Fig. 1D), suggesting specificity. Ndel1, DID (derived from Ndel1) and the Nde1-DID peptide pulled down dynein intermediate chain (DIC), whereas no signal was noticed with either pep3 or the control GST peptide. Similar results were obtained using extracts of HEK293 or COS-7 cells. The interaction between Ndel1 with pep3 in a cell lysate was enhanced when Ndel1 was palmitoylated (Fig. 1E). Ndel1 and pep3 can interact directly as demonstrated by a GST pull down experiment, whereas GST-pep3 pulled down 6 × His Ndel1 but the GST protein did not (Fig. 1F). Furthermore, pep3 can self-interact since GST-pep3 pulled down 6-His-pep3, but GST did not (Fig. 1G). The DID peptide pulled down detectable amounts of dynein heavy chain and dynein intermediate chain identified by mass-spectrometry sequencing of the indicated bands (Fig. 1H). Our results indicate that the DID peptide interacts with dynein (therefore named Dynein Interacting Domain) and pep3 is an additional Ndel1 self-association domain, which is sensitive to the palmitoylation status of Ndel1.

The squid genome is not yet available, however, it has been shown to contain multiple molecular motors including cytoplasmic dynein and members of the kinesin superfamily of proteins, which exhibit high degree of similarity to the mammalian ones (Degiorgis et al., 2011). Although the Ndel1 ortholog has not been detected in squid so far, the squid genome is likely to contain one based on Western blot analysis (Fig. 1I). Using polyclonal anti-Ndel1 antibodies we detected a cross-reactive band in a protein lysate from the squid axoplasm (Fig. 1I). This band has the same molecular weight as Ndel1 detected in a mouse brain protein lysate (Fig. 1I). Furthermore, our previous bioinformatic analysis revealed that Ndel1 and Nde1 are highly conserved proteins (Shmueli et al., 2010). Nevertheless, our interpretation of the results will include the possibility that the squid genome does not contain an ortholog of Ndel1.

We further examined whether Ndel1 and its related peptides may interact with conventional kinesin using far-Western analysis (Fig. 1J). The different tested proteins of kinesin included $\alpha 2\beta 2$ that is the recombinant wild-type kinesin consisting of two heavy chains and two light chains, $\alpha 2$ is kinesin heavy chain homodimer and ΔTail is kinesin heavy chain deleted after residue M559. Our results indicate that the tested Ndel1/Nde1-derived peptides interacted with all the tested kinesin proteins whereas the GST control did not. We are not sure what are the functional implications of these interactions since NDEL1 did not activate kinesin in single-molecule assays.

To evaluate the role of Ndel1 on transport in vivo, we injected either GST, GST-Ndel1 (Ndel1), GST-Ndel1-DID (DID), the related peptide from Nde1 (Nde1-DID) and GST-pep3 (Pep3)

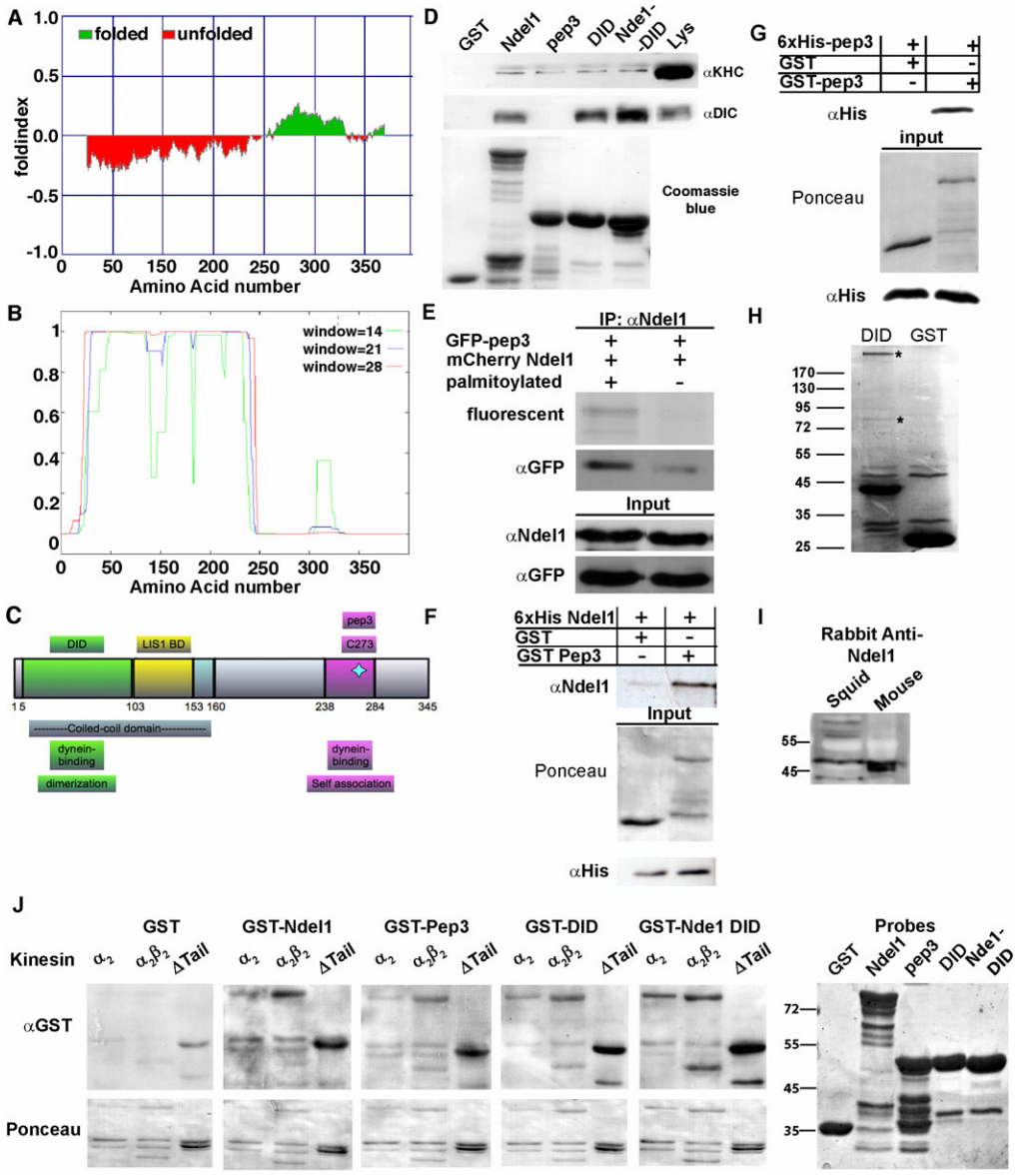

Fig. 1. Ndel1 and Nde1 derived peptides. (A–B) Predicted domains in Ndel1, X axes are residue numbers. **(A)** Ndel1 is an unfolded protein. **(B)** The N-terminal of Ndel1 is predicted to form coiled-coil structures. **(C)** Schematic presentation of Ndel1 and the derived peptides. **(D)** GST-pull down from brain lysate. GST-Ndel1, pep3, DID and Nde1 pulled down kinesin heavy chain (KHC), (top panel), and with the exception of pep3 they pulled down dynein intermediate chain (DIC) (middle panel). The proteins used for pull-down experiments are visualized by Coomassie blue staining (bottom panel). **(E)** Palmitoylated mCherry-Ndel1 (left lane) preferentially interacts with GFP-pep3 in a cell lysate (left lane second panel from the top in comparison with the right lane. Similar amounts of the proteins were detected by Western blot (Input). **(F)** Ndel1 and pep3 interact directly. GST-pep3 pulled down 6 × His Ndel1, whereas GST did not (top blot). Similar amounts of proteins were noted in the input: GST was detected with Ponceau S stain and 6 × His Ndel1 was detected with anti-His antibody. **(G)** GST-pep3 pulled down 6 × His-pep3, whereas GST did not (top blot). The amounts of the input proteins were detected either by Ponceau S staining (middle panel) or by anti-His tag blotting (bottom panel). **(H)** Ndel1-DID peptide pulled down dynein heavy chain and dynein intermediate chain (the proteins identified by mass-spectrometry are indicated by asterisks), whereas GST did not (left lane). **(I)** Rabbit anti-Ndel1 antibodies detect a cross-reactive protein in the squid axoplasm protein lysate (first lane) of similar molecular weight to the one detected in a mouse brain protein lysate (second lane). **(J)** Interaction of Ndel1 and peptides with conventional kinesin. GST Ndel1, GST pep3, GST DID and GST Nde1 DID interact with recombinant kinesin constructs α_2,$\alpha_2\beta_2$ and ΔTail (α2 is kinesin heavy chain homodimer, α2β2 is the recombinant wild-type kinesin consisting of two heavy chains and two light chains and ΔTail is kinesin heavy chain deleted after residue M559) shown in the upper panel with anti GST. The amounts of recombinant kinesin proteins are presented in lower panel with Ponceau S staining of each membrane. The probes that were used are shown in the right gel image by Coomassie Brilliant Blue staining.

mixed with 100 nm diameter carboxylated fluorescent beads into the giant axon of the squid (Fig. 2A–B). Transport of the fluorescent beads was monitored using confocal microscopy (supplementary Movies 1–3) (Fig. 2C–D). Movements of the fluorescent beads were analyzed using the automatic spots-tracking module of the Imaris software package (Bitplane, Inc.) to generate a set of position lists. The generated lists consisted of a track index, followed by x and y coordinates and a time stamp. The deduced tracks enabled to resolve the direction and velocity of each bead during each captured time frame. The anterograde direction was given a positive sign while the retrograde direction has a negative sign.

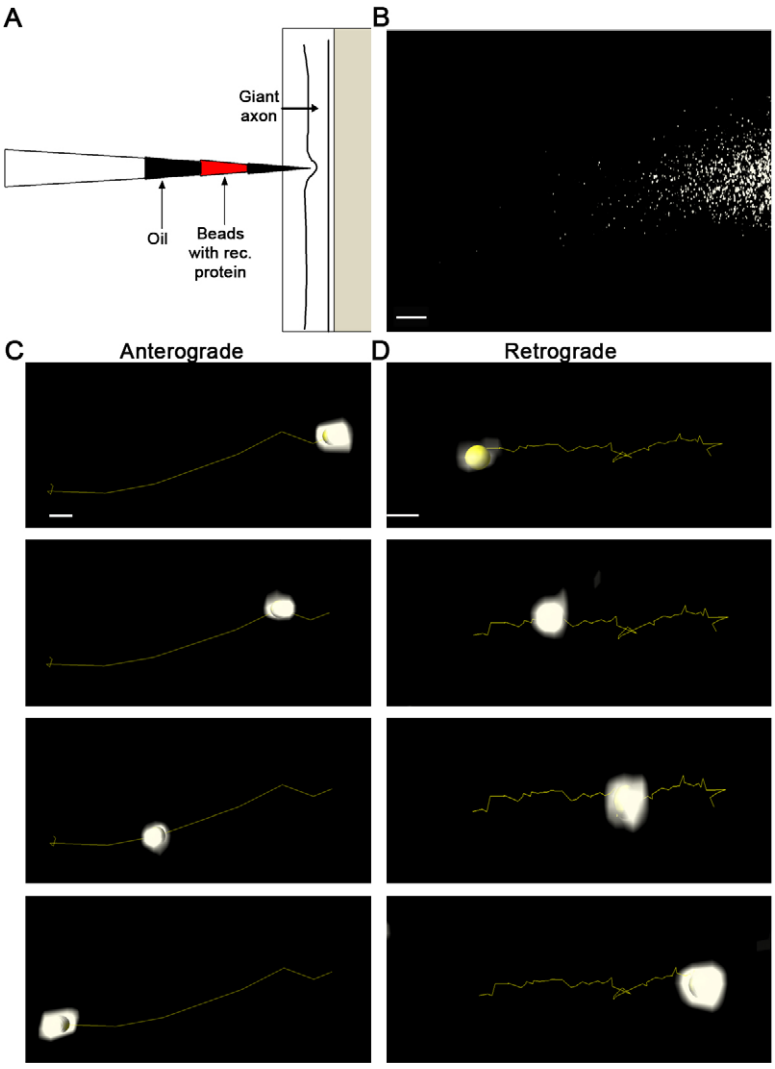

Fig. 2. Injection of peptides mixed with carboxylated beads into the squid giant axon. (A) Schematic presentation of the injection procedure. A dissected axon was placed on a glass slide, where the suspension of peptides and beads between two oil droplets were injected. **(B)** Image of the beads in the axon (x40 lens). **(C)** The panel shows a sequence of time frames capturing an individual bead moving in the anterograde direction. **(D)** The panel shows a sequence of time frames capturing an individual bead moving in the retrograde direction. Size bars: B, 10 µm; C and D, 0.5 µm. See also Table 1 and supplementary Movies 1–5.

Each experiment was conducted in 4–6 different axons, recorded at 4 sec intervals for 100 frames. The motile beads were tracked resulting in 1194–4046 tracks. The tracks were separated into segments that were defined by continuous movements of a bead in one direction (4765–12324 segments per treatment). The movements from one frame to the next were used to calculate instantaneous movements (20,304–49,640 per treatment). The summary of the data is shown in Table 1. A few representative tracks are shown in Fig. 3A. Beads appear and disappear as they enter and leave the focal plane. Some beads moved in one direction only, along with pauses of zero velocity (the green, turquoise and purple traces, Fig. 3A). Other beads changed directions, either with or without intervening pauses (the red and blue traces, Fig. 3A). Thus several tracks include both anterograde and retrograde segments. We noticed a large variability of the velocity within the individual segments; beads were often accelerating or slowing down even while moving in one direction. To distinguish the effects of the various peptides on motor-induced bead motion a number of statistical tests to the data were applied. First, we compared the individual, instantaneous movements at the measurement interval from the four treatments in comparison to GST (Fig. 3B–E). The

Table 1: Summary of data derived from the experiments conducted in the giant axon of the squid. Tracks were defined when individual beads could be followed for at least three time frames. Segments were derived from the tracks that were split when a bead stopped or reversed its orientation. Points indicate the individual data points composing the instantaneous movements of beads derived from the tracks.

Treatment	no. of Axons	Tracks	Segments	Tracked Points
GST	4	1194	4765	20304
GST-Ndel1	6	3079	12324	45794
GST-pep3	5	3266	9127	47775
GST-DID	4	4046	9679	49640
GST-Nde1-DID	5	2109	6667	28308

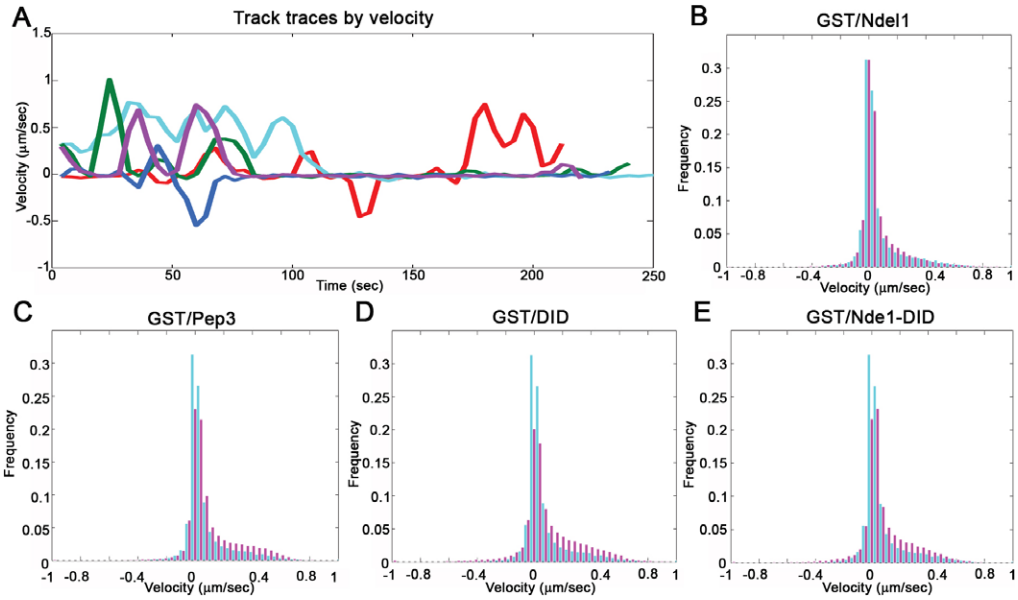

Fig. 3. (A) Directed velocity of representative tracks along time (x axis time in seconds, y axis velocity in μm/second). Example of five individual long tracks over time, each track is shown in a different color. Note that there are fast and slow movements both in the anterograde (positive sign) and retrograde (negative sign) directions. **(B–E)** Frequency distribution of instantaneous velocities in all tracks, the distribution of velocities for the control peptide GST (turquoise) is shown in all. The different peptides are shown in pink. The x axis is velocity in μm/second and y axis is the fraction of movements at a specific velocity. The peptides affect the distribution of instantaneous velocities.

histograms have been normalized to the same areas, so that heights of the bars can be interpreted as probabilities. The horizontal axes show velocities in units of microns per second. The GST control appears in turquoise in all panels for comparison. The first and most notable feature is that there are no peaks at the canonical free motor velocities, which we would expect to be approximately 0.5∼1 μm/sec based on in vitro measurements (Howard et al., 1989; King and Schroer, 2000; Toba et al., 2006; Vale et al., 1996). Instead there is a tall central peak at zero, surrounded by a broad shoulder to the anterograde side and a slim shoulder to the retrograde side. These shoulders decay to a maximum velocity of approximately 1 μm/sec in both retrograde and anterograde directions, just where we might have expected to see peaks due to single motor activity. The shoulders are not symmetric, but show a skew toward the anterograde direction. This is consistent with the visual observation that the cloud of injected beads moves and spreads mainly toward the axon tip, away from the cell body. Overall, the instantaneous velocities are much smaller than expected from in vitro motility assays. This might indicate a drag against the motion, or the effect of competing motors. Subtle differences appear in the shoulders of the distributions with the various peptides. Specifically, the full-length Ndel1 protein increased instantaneous velocities slightly in the anterograde direction (Fig. 3B), while the DID and Nde1-DID peptides increased the instantaneous velocities in both directions with respect to the GST control (Fig. 3D,E). Pep3 had a more pronounced effect in comparison with that of full-length Ndel1, namely it increased the velocity of anterograde steps without an effect on the retrograde steps (Fig. 3C). Furthermore, addition of the peptides, but not of the full-length Ndel1, significantly reduced the number of immobile beads (Fig. 3C–D and Table 2). DID had the most pronounced effect in this regard and its addition decreased the percentage of paused beads from 58% to 38%. Addition of Pep3 or Nde1-DID resulted in 45% of paused beads in comparison with 58% with the GST control. As a quick test of significance we split each of the datasets into six random sub-groups and confirmed that the visual differences remained qualitatively unchanged among them. In order to confirm quantitatively that GST and treatment step velocity distributions are distinct, we applied the Kolmogorov-Smirnov test, which yielded extraordinarily small p values ($<10^{-21}$).

The recorded tracks were further divided into retrograde and anterograde segments; when the movement of the bead stopped or changed direction a new segment was defined. To demonstrate the differences in the distributions of the segments more effectively we turned to a two-dimensional, color-based presentation (Fig. 4). For each treatment the segment duration (in seconds) is plotted along the x-axis, and the directional run length (in microns) along the y-axis. These plots show the correlation between persistence in length and temporal duration. In particular, each point in 2D shows the total length and duration of the segments it represents and the coloring represents the percentage of the segments with the particular duration and velocity. This presentation contains more information than conventional bar histograms as it shows how the segment lengths depend on their duration. We see clearly that anterograde segments are more numerous than retrograde in the GST control

Table 2: Percentage of paused beads. The percentage of paused beads (two bins located at –0.02 and 0.02 μm/sec shown in Fig. 3B–E) was derived.

Treatment	Percentage of total beads −0.02 μm/sec bin	Percentage of total beads 0.02 μm/sec bin	Percentage of paused beads
GST	31	27	58
GST-Ndel1	31	24	55
GST-Pep3	23	22	45
GST-DID	20	18	38
GST-Nde1-DID	22	23	45

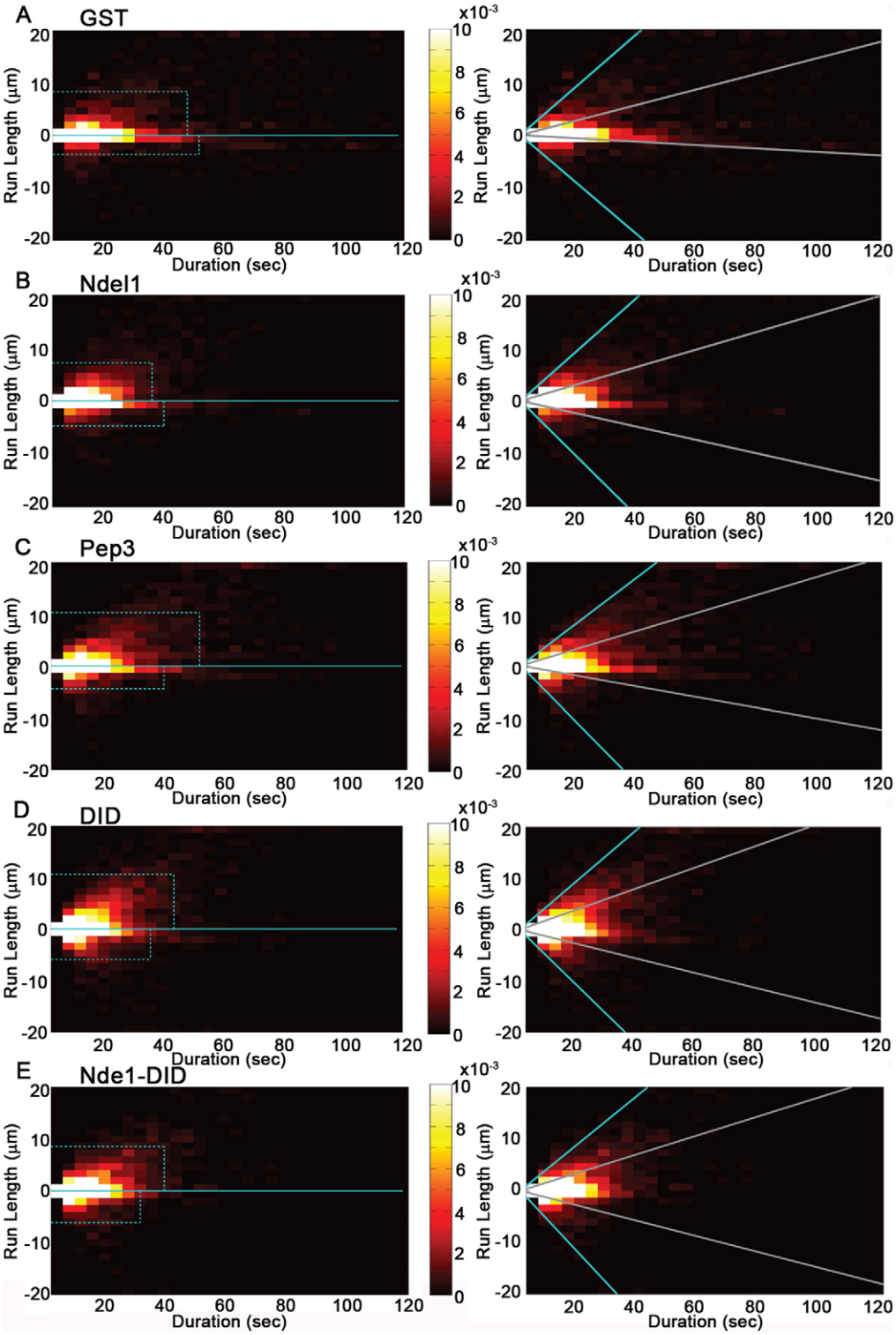

Fig. 4. Segments analysis. The segments were plotted on a 2D heat map, where the x axis indicates the duration in seconds and the y axis indicates the total run length in microns. Negative y values are attributed to retrograde directed segments and positive y values are attributed to anterograde directed segments. The colors of the 2D heat map reflect the number of segments, the number color relation map is shown in each row. Dashed lines indicate the position of the 85% limit of the segments (left). The position of the median values of retrograde or anterograde segments is indicated by the grey line, whereas the turquoise line represents the 95% limit (right). **A)** GST. **B)** GST-Ndel1. **C)** GST-Pep3. **D)** GST-DID. **E)** GST-Nde1-DID.

and in all treatments (about 2/3 of the total segments following exclusion of the very short segments, Fig. 4A left panel). In order to emphasize the differences, thin lines were drawn over the 2D plots representing bounds of 85% in the distributions of both length and duration of continuous runs (Fig. 4 left panels). A shift of the vertical line to the left indicates that a persistent motion is shorter on average; while the vertical position of the two horizontal lines indicates represents the segment lengths in either direction. The intersections of the horizontal and vertical lines with the y and the x axes indicate the duration of segments and the displacement of the segments and their confidence interval are shown in Table 3. The duration of segments in the anterograde direction was slightly affected by the treatments. It shortens in the presence of full length Ndel1 and extended a little

Table 3: Summary of time and displacement intercepts and interval from 85% cutoff presented in Fig. 4 left column as well as average velocities (μm/sec) of 95 or 50 percentile of anterograde or retrograde segments presented in Fig. 4 as well as average velocities normalized to GST.

	GST	Ndel1	Pep3	DID	Nde1–DID
Time (sec)					
Antrograde	48.00 (44–52)	36.00*** (36–36)	52.00 (48–52)	44.00* (40–44)	40.00*** (36–44)
Retrograde	52.00 (48–60)	40.00*** (36–44)	40.00*** (40–44)	36.00*** (36–40)	32.00*** (28–36)
Displacement (μm)					
Antrograde	8.60 (7.8–9.6)	7.50 (6.9–8)	10.60** (9.8–11.4)	11.00*** (10.4–11.5)	8.90 (8.2–9.8)
Retrograde	3.70 (3.3–4.6)	4.80** (4.5–5.2)	4.60 (4.2–5.1)	6.10*** (5.7–6.7)	6.30*** (5.6–7.1)
Average velocities (μm/sec)					
Anterograde 95%	0.5 (0.45–0.55)	0.51 (0.48–0.54)	0.45 (0.43–0.47)	0.51 (0.48–0.54)	0.48 (0.45–0.52)
Retrograde 95%	0.49 (0.43–0.65)	0.57 (0.54–0.57)	0.6 (0.53–0.65)	0.58 (0.53–0.64)	0.63 (0.57–0.68)
Anterograde 50%	0.15 (0.13–0.16)	0.17 (0.15–0.18)	0.18*** (0.17–0.18)	0.21*** (0.20–0.22)	0.18*** (0.17–0.19)
Retrograde 50%	0.033 (0.03–0.04)	0.13*** (0.11–0.14)	0.1*** (0.09–0.13)	0.15*** (0.13–0.16)	0.15*** (0.13–0.17)
Average velocities normalized to GST as 1					
Anterograde 95%	1.00	1.02	0.90	1.02	0.96
Retrograde 95%	1.00	1.16	1.22	1.18	1.29
Anterograde 50%	1.00	1.13	1.20	1.40	1.20
Retrograde 50%	1.00	3.94	3.03	4.55	4.55

*p-value <0.01
**p-value <0.005
***p-value <0.001

with pep3 addition. All treatments decreased the duration of the retrograde segments, mainly Nde1-DID and DID. The displacement of the retrograde tracks was increased in all the treatments, where the most evident effects were noted following addition of DID and Nde1-DID.

In addition, we examined the average velocity per segment. The peak follows the lightest-colored ridges in Fig. 4 (right panels). The diagonal bounding lines are drawn to include 95% of the distributions (turquoise) and the median, 50% (grey). The median shows us the typical or most probable value, while the limit shows the average velocity of the fastest segments. All points that lie along a diagonal line starting from the origin have the same ratio of length to duration, so the slope represents a similar average velocity within the segments. The average velocities and their confidence interval were calculated at the 95% and 50% criteria (Table 3), and were normalized in relation to the retrograde or anterograde average velocities of control GST treated segments (Table 3). Overall, the effect of the peptides was more pronounced when the median velocities are inspected in comparison to the 95 percentile. All of the treatments increased the median velocities of the retrograde segments where DID and Nde1-DID exhibited a 4.5 fold increase in comparison with GST whereas the duration decreased (Table 3). In addition, all of the treatments resulted in increased velocities of the anterograde segments. A modest increase was noted when Ndel1 was added (13%), Pep3 and Nde1-DID each increased the anterograde velocities by 20% and DID contributed additional 40%.

Discussion

A model for bidirectional transport

How balanced bidirectional transport is generated in vivo is a topic of active investigation and several possible models have been proposed (Gross, 2004; Muller et al., 2008). There may be a mechanical competition that leads to temporary domination of one motor family over the other. In the "tug of war" model, for example, several motors of both polarities are available to engage the microtubule tracks. In balance the two types will cause a stall. If one side begins to detach, however, the fewer opposing motors remaining will require less and less force to detach one by one. This generates a detachment cascade that leads to one motor family dominating the motion at a time. Our data suggest a model in which oppositely directed motors remain engaged with the microtubules simultaneously. One side dominates the motion, while motors in the opposing direction confer a drag. This is consistent with the slow velocities we observe compared to in vitro studies. Our results fit well with previously measured velocities of negatively charged fluorescent beads in the squid axon. Previous publications measuring movements of beads in the squid axon have using manual tracking and noted that the average velocity was 0.02 μm/sec and the maximum velocity was 0.4 μm/sec (Terada et al., 2000; Terasaki et al., 1995). A recent article, which analyzed movements of PrP^c vesicles in mammalian hippocampal axons demonstrated that particles moving in the retrograde direction had shorter mean run lengths than those moving in the anterograde direction (4.8 versus 6.2 μm) (Encalada et al., 2011). Our results also demonstrate a reduced displacement for retrograde segments (3.7–6.3 versus 7.5–11 μm, Table 3). In addition, the kinetics of cargoes transported within an axon as well as the anterograde bias of this population in mammalian axons fitted the slow motility in our observed large scale tracking of individual beads (Scott et al., 2011). In the context of molecular motors, movement involves unit steps between structurally fixed binding sites along the microtubule. Free-running, the ATP turnover rate determines the maximal velocity as a stepping frequency. An opposing force, or drag, cannot change the step size, but rather affects strongly the time interval between steps, resulting in a reduced velocity. In our observations, the motor

movements in both directions show large variation in velocity within a single track. Typically, the beads are not moving at constant velocity as would be expected from motor activity in vitro; rather they are accelerating or slowing down. Stall periods may represent a rigor state with both motors attached but unable to move. This is equivalent to a tug of war model in which the detachment cascade is not complete, perhaps a "kick and scream" variant to represent the competition before one side wins, as shown in Fig. 5. We will discuss below how Ndel1 related peptides affect bidirectional transport within this model.

Bidirectional transport and motor regulation

In addition to force-based competition bidirectional transport may involve specific regulation of the motors themselves. Motors may be composed of different isoforms (King et al., 2002; Myers et al., 2007), they may be modified following translation (Song et al., 2007; Vaughan et al., 2001) and the interactions between the different motors and other regulatory molecules may vary (Ligon et al., 2004). The motor modifiers may have a direct effect on ATPase activity and force generation. Alternatively, they may affect the strength of motor interaction with microtubules, or the interactions between the motors and the various cargoes. Post-translational modifications of tubulin or binding of other microtubule associated proteins (MAPs), such as tau, may also affect the binding of motors to the tracks in a differential manner (Dixit et al., 2008; Dompierre et al., 2007; Erck et al., 2005; Ikegami et al., 2007; Mandelkow et al., 2004; Peris et al., 2006; Reed et al., 2006; Seitz et al., 2002). A few molecules are known to interact with different motor families and to affect their activity (Gross et al., 2002; Kardon and Vale, 2009). One such example is dynactin, an integral component of the dynein motor that allows it to bind a variety of cargoes, regulates its activity directly, and enhances its processivity (Schroer, 2004; Vallee et al., 2004). In addition, dynactin interacts with kinesin-2 and kinesin-5, two plus end-directed microtubule motors (Berezuk and Schroer, 2007; Blangy et al., 1997; Deacon et al., 2003). Dynactin coordinates between dynein and kinesin activities in several systems (Deacon et al., 2003; Gross, 2003; Haghnia et al., 2007; Martin et al., 1999).

Ndel1 and Nde1 are best known for their interaction with cytoplasmic dynein and LIS1 (Feng et al., 2000; Niethammer et al., 2000; Sasaki et al., 2000), through which they mediate their effects on dynein and retrograde transport (Feng and Walsh, 2004; Liang et al., 2004; McKenney et al., 2010; Shim et al., 2008; Stehman et al., 2007; Yamada et al., 2008; Yan et al., 2003; Zhang et al., 2009). We identified dynein-binding activity in the N-terminal DID domain and the addition of this peptide enhanced retrograde movements but the duration decreased. This activity may require dimerization properties embedded within the domain that were defined in structural and interaction-based studies (Bradshaw et al., 2009; Derewenda et al., 2007). An independent recent study demonstrated that the first eighty amino acids of Ndel1 (included in DID) binds directly to dynein intermediate chain and is essential for spindle pole organization in *Xenopus* egg extracts (Wang and Zheng, 2010). An additional recent study also demonstrated dynein binding activity in the first ninety-nine amino acids of Ndel1 and also Nde1 and further demonstrated that the interaction with dynein is regulated by phosphorylation in the C-terminus (Zylkiewicz et al., 2011). Therefore, even if the squid genome does not contain an ortholog of Ndel1 (which we believe is unlikely), the introduced DID peptide is likely to bind to the squid cytoplasmic dynein molecular motor which is similar

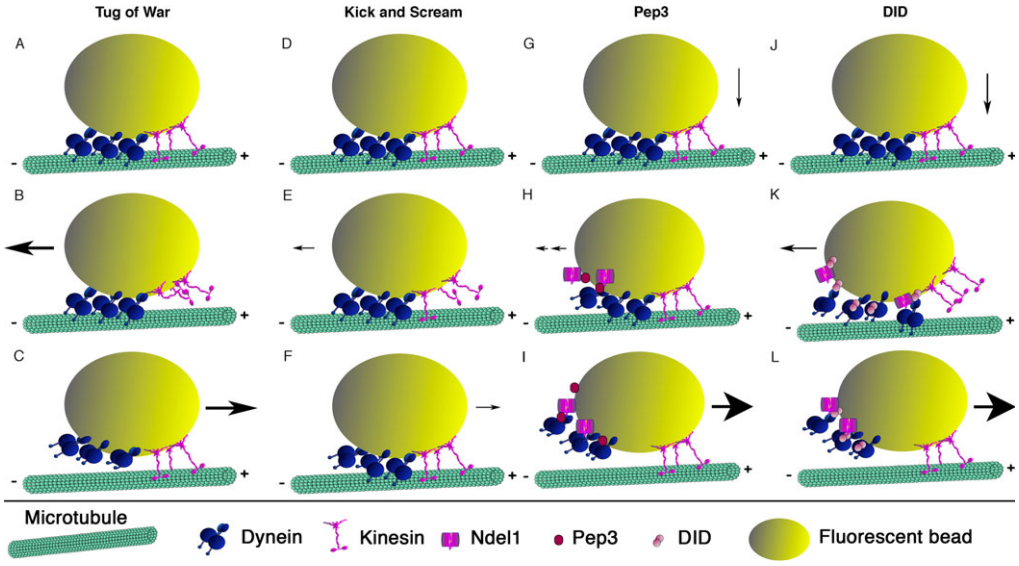

Fig. 5. A bidirectional transport model as a generalization of the tug of war model. (A–C) Tug of war model. **(D–F)** Kick and scream model. **(G–I)** Addition of pep3. **(J–L)** Addition of DID. **(A, D)** An equal numbers of motors (or unequal numbers that generate equal forces) are attached to the microtubule and pull in opposite directions. This should generate a stall condition, which we observe as the tall peak at the origin in the displacement histograms of Fig. 3. **(B,C)** A fluctuation in the number of motors may lead to a detachment cascade, leaving the dominant side unopposed to move at full velocity. **(E,F)** To the extent that opposing motors may reattach, even transiently, they hinder the motion by making forward steps less frequent, resulting in a lower observed velocity. One side is fighting the other still attached, we call this regime "kick and scream". **(G, J)** Addition of pep3 or DID enhance motility. **(H)** Pep3 may recruit cytoplasmic Ndel1 and other factors resulting in some enhancement of retrograde motility. **(I)** Pep3 binding to Ndel1 may result in inactivation of cytoplasmic dynein and enhancement of anterograde movements. **(K)** DID binds to Ndel1 and also to cytoplasmic dynein resulting in faster retrograde motility. **(L)** DID's binding to Ndel1 and to cytoplasmic dynein results in activation of anterograde movements.

to the mammalian one (Degiorgis et al., 2011). The second domain studied here, pep3 (amino acids 256–291), exposed a new dimerization domain that is sensitive to protein palmitoylation. If the squid does not contain an ortholog of Ndel1 we must speculate that the observed effects are due to some unknown protein-protein interactions. In addition, our results indicated that all the peptides used in this study are capable of forming a complex with conventional kinesin though the functional results of these interactions are not clear.

Treatment with Ndel1-derived peptides may affect the competition between dynein and kinesin in a number of ways: they may affect one or the other motor directly, they may affect the strength of the motor interaction with microtubules, or they may affect the strength of the motor interaction with the bead cargo. A telling observation lies in the position traces of Fig. 3A. Some tracks show movements in one direction only, along with pauses of zero velocity. Other traces show movements that pass smoothly through zero velocity, i.e., they slow down and reverse direction continuously without an intermediate stall. This observation is hard to reconcile with a model explaining bidirectional transport by strict alternation of kinesin and dynein motor activity. It would be a natural outcome of competition in which both motors remain engaged, at least transiently, during the excursions in either direction. Progressively increasing velocity would be a result of progressive detachment of opposing motors, while attachment of opposing motors would decrease the velocity. It is significant in this regard that those reversals in direction may or may not involve an intermediate stall.

Surprisingly, our results show that Ndel1 related peptides enhance primarily the anterograde movements of the negatively charged beads. The major influence on anterograde movement was unanticipated given that Ndel1 interacts directly with dynein, yet the anterograde enhancement appears in many aspects of the motion. When looking at the distribution of instantaneous movements we see a relative increase in the number of anterograde steps. This increase comes primarily at the expense of stall periods; the length distribution of individual retrograde steps weakly affected if at all. Furthermore, we see an enhancement of anterograde persistence. By bounding the segment distributions at 85% of each population, we see an increase in overall length of the anterograde movements under DID and Pep3 treatments. Interestingly, the full-length Ndel1 protein did not have a strong effect in most of the examined aspects. We assume that this is due to the fact that Ndel1 is overall an unstructured protein and its activities are exposed when it is found in the appropriate protein complexes. Dynamic post-translational modifications such as phosphorylation and palmitoylation are likely to play an important role in determining which protein complexes Ndel1 will participate. The retrograde segments were affected in a different way. All treatments decreased the duration of movements, while the displacement increased most following addition of DID and Nde1. Finally, there was an increase in both median and maximal average velocities per segment following all treatments in the retrograde direction, and in the median in the anterograde direction. This finding points to enhancement of some parameters relating to both motors. The most dramatic effects are observed in the velocities of the segments in the retrograde direction. The average control velocity is very slow and following the treatments increased 3–4.5 fold. This may hint to a distinct mechanism of action of the added peptides on the different motor proteins.

In this case how the Ndel1-derived peptides affect bidirectional transport may be interpreted that an inhibition of dynein attachment or stroke would appear as an enhancement of anterograde movement. We distinguish between the effects of pep3 and DID. Our data suggests that pep3 may affect anterograde and retrograde movements indirectly via the interaction of the pep3 peptide with Ndel1 (Fig. 5G–I). As mentioned above, in case that the squid does not contain an ortholog of Ndel1, the effects will be mediated through other, currently unknown protein interactions. The DID peptide has the capability to interact both with Ndel1 and directly with cytoplasmic dynein (Fig. 5J–L). As such, it may possibly enhance dynein's activity or affect the number or conformation of engaged retrograde motors. Accumulating data suggest that changes in the number of actively engaged motors directly affect the motility and directionality of different cargoes (Ally et al., 2009; Encalada et al., 2011; Hendricks et al., 2010; Shubeita et al., 2008). Nevertheless, the main consequences following reduction of the levels of either dynein or kinesin were decreases in the length of bidirectional runs, and increases in pause frequencies, consistent with down-regulation of opposing motor activity. Surprisingly however, mean segmental velocity, a parameter also influenced by motor activity, was largely unaffected (Encalada et al., 2011). Our study also suggests that active bidirectional motors are moving one cargo where each movement results from the net competition between the motors, which was displayed as a modified version of the "tug of war", namely, "kick and scream". Furthermore, our study demonstrated how additional regulatory proteins may affect retrograde and anterograde transport in a different way than directly affecting the number of motors. Addition of the peptides decreased the number of paused beads and increased the average velocities both in the anterograde and retrograde direction. Run length in the anterograde direction was largely unaffected, whereas in the retrograde direction it was shortened. Thus, our study shows an in vivo demonstration how bidirectional transport can be regulated using motor-binding proteins.

Materials and Methods

Squid axon injection

The back stellar nerve or giant axons were dissected from squid (*Loligo pealleii*) in running sea water. The axon was moved to calcium free seawater, surrounding fibers and connective tissues were removed using a stereomicroscope. Injections were assisted with a micromanipulator (Narishige SM20, Model SM-20) using pulled glass pipettes filled with a mercury drop attached to a Micrometer syringe (Gilmont S-1200, GS-1200). FluoSpheres® Fluorescent Microspheres (Molecular probes, Invitrogen, Carlsbad, CA) carboxylate-modified, 0.1 µm, red (580/605) were washed using Microcon YM-30 filter tubes (Millipore, Billerica, MA) with double-distilled water by centrifugation at 13,000 g, for 3 minutes at room temperature. The fluorescent beads were retrieved by inverting the filter followed by centrifugation at 1000 g for 3 minutes at room temperature. Double-distilled water was added to restore the initial volume, the protein was diluted in 1 × PBS. Beads were mixed 1:1 with the recombinant proteins up to thirty minutes prior to the injection (3.85×10^{-6} % of the carboxylated binding sites on the beads are occupied by the recombinant protein, based on the assumption that one binding site can bind one protein molecule). All recombinant proteins and peptides were tagged with GST and identical molar quantities were taken for injection. Each beads:protein sample was loaded onto the injection pipette between the two oil droplets (Dimethylpolysiloxane, Sigma-Aldrich, St. Louis, MO) which were used for marking the injection point, monitoring the injection stability and preventing the penetration of sea water into the axoplasm. The axon and the injection pipette were placed on a stage of a regular up right light microscope (Axiscope, Carl Zeiss Inc., Thornwood, NY), the tip of the injection pipette was placed in close vicinity to the membrane of the axon. The pipette is then inserted into the axoplasm and the oil and the sample were injected into the middle of the axoplasm. The injection

occurred 12–15 minutes after axon retrieval, after which the axon was placed onto a cover slip suitable for confocal microscopy imaging.

Imaging

Imaging was done on a LSM 710 confocal microscope (Carl Zeiss Inc., Thornwood, NY) using channels; DIC (differential interference contrast) and a fluorescent channel (excitation 594 nm, 3% intensity, 597–677 nm filters). The injection spot was located using a 10× objective. Fluorescent beads were imaged using a 40× objective (LD C-Apochromat 40×/1.1 W korr, pixel size x, y 0.131203 μm), where frames were captured every 4 seconds one hundred times similar to previously described conditions (Satpute-Krishnan et al., 2006) and re-analyzed (Vermot et al., 2008). The first time-lapse series from each axon was analyzed.

Imaris analysis

Movements of the axon over time were corrected using the AutoAligner software (Bitplane Inc., Zurich, Switzerland) by aligning the oil bubble indicating the injection site. The movements of the fluorescent particles were analyzed using the automatic spots-tracking module of the Imaris software package to generate a set of position lists (Bitplane Inc., Zurich, Switzerland). The diameter of the spots was measured as an average of 0.4 micron and the threshold filter used was the spot quality. Tracks were generated using the autoregressive motion algorithm using 5 micron maximal distance and no gap allowed. Tracks appeared shorter than 3 frames or those exhibiting a high y displacement value and make few steps only in the y axis (track AR1 Y filter) were eliminated. Note that a track as recognized by the software may consist of several segments moving back and forth, until the particle moves out of the plane of focus and disappears. Following automated tracking, artificial tracks were removed manually from the data set.

Statistical analysis

All statistical analysis, histograms and heat maps were done by Matlab software (R2009a, The MathWorks, Natick, MA). Track traces were done by plotting directed velocities in the y axis and time in seconds on the x axis. Instantaneous velocities were analyzed using velocity data for each bead in each time frame. Positive values represent anterograde movements and negative values represent retrograde movements.

Histogram plots of velocity values for each treatment were generated by binning velocity values into equally spaced intervals of 0.04 μm/sec and normalized to an area of 1.

The track traces were split into the anterograde and the retrograde segments. The end of each segment was defined by either stop or change of direction of the movement. Run length and the duration of each segment were binned into two-dimensional histogram and shown as a heat map: x axis represents segment duration in seconds and y axis represent total run length in microns. The coloring represents the relative abundance of segments with the designated run length and duration, ranging from zero in black to 1% colored white.

85% cutoffs for run length and segment duration were calculated separately after excluding the segments that belong to bins with more than 1% of the data (normally segments with a close to zero run length).

To calculate the median and 95-quantile velocities we excluded the segments with a close to zero run length and calculated the average velocity for each of the remaining segments. p-values for cutoffs were estimated by bootstrapping with re-sampling and with replacement.

GST pull-down

GST proteins were isolated from bacteria and purified on glutathione agarose according the manufacturer's instructions (Sigma-Aldrich, St. Louis, MO). Recombinant proteins (5 μg) were incubated with freshly prepared brain lysate, cell lysates or other recombinant proteins for 2 hours using slow rotation at 4℃. Lysate were prepared by homogenization of brain or cells in Tris-Triton buffer (20 mM Tris pH 8, 100 mM NaCl, 1 mM EDTA, 0.1% Triton with protease inhibitor). After two hours washed glutathione agarose beads were added and incubated for another hour at 4℃. The agarose beads were pelleted in a centrifuge at 2400 g for 5 minutes and washed three times. Following the third wash 2× protein sample buffer was added to the pellet and the samples were heated to 95℃ for five minutes. Proteins were separated on 10–12% SDS-PAGE acryl amide gels and either transferred to Nitrocellulose membranes for Western blotting or stained directly with Coomassie Brilliant Blue (Sigma-Aldrich, St. Louis, MO) for mass spectrometry identification. Antibodies used for Western blot analysis included anti kinesin heavy chain (Millipore, Billerica, MA) and anti-dynein intermediate chain (Santa Cruz Inc., Santa Cruz, Ca). Loading control of GST proteins is done by ponceau staining of membrane, all other proteins were checked with specific antibodies (anti-Ndel1, Anti-GFP and Anti His) indicated as "input".

Palmitoylation of Ndel1 and binding of pep3

Palmitoylation of Ndel1 was followed using metabolic labeling with 17-Octadecynoic acid (17-ODYA, Cayman Chemical, Ann Arbor, MI) of HEK293 cell line over expressing mCherry-Ndel1, GFP-pep3 with or without HA-DHHC7 (Martin and Cravatt, 2009). Cells were metabolically labeled by addition of 25 μM 17-ODYA to the media eight hours after calcium-phosphate transfection for overnight. Following which, cells were washed and lysed. Ndel1 was immunoprecipitated with rat anti-Ndel1 antibodies (received from Dr Aoki, Tokyo University) as previously described (Shmueli et al., 2010). The immunoprecipiate was subjection to click chemistry which involved the addition 1 mM Tris (2-arboxyethyl) phosphine (TCEP, Sigma-Aldrich, St. Louis, MO) dissolved in water, 100 μM Tris [(1-benzyl-1H-1,2,3-triazol-4-yl) methyl] amine (TBTA, Sigma-Aldrich, St. Louis, MO) dissolved in DMSO/t-butanol (20%/80%), 1 mM CuSO4 and 20 μM Azide modified Alexa Flour® 647 (655 emission/650 excitation Molecular probes, Invitrogen, Carlsbad, CA) in PBS. Reaction was left on the bead-proteins complex for one hour at room temperature and then washed. Proteins were separated from beads to 2× protein sample buffer by heating to 95℃ for five minutes followed by SDS-PAGE. Gels were scanned for a fluorescent signal with Typhoon™ 9400 (GE Healthcare Bio-Sciences Corp., Piscataway, NJ) 670 emission/633 excitation. Western blots were conducted using Rat anti Ndel1 and mouse anti GFP (Sigma-Aldrich, St. Louis, MO).

Far Western

His-tag conventional kinesin proteins previously described (Coy et al., 1999) were isolated from bacteria and purified using HisPur™ Ni-NTA Resin (Thermo scientific). Three constructs were used: full length kinesin heavy chain homodimer (α_2), the recombinant wild-type kinesin consisting of two heavy chains and two light chains ($\alpha_2\beta_2$) and delta-tail construct which is kinesin heavy chain deleted after residue M559. Five microgram of each protein were separated on 10% SDS-PAGE and transferred onto a nitrocellulose membrane. The membranes were then incubated with declining concentrations of guanidine-HCl (6M, 3M, 1M and 0.1M) in AC buffer (10% glycerol, 100 mM NaCl, 20 mM Tris pH 7.5, 1 mM EDTA, 0.1% Tween-20) with 2% milk and 1 mM Dithiothreitol for 30 minutes for each concentration. Blocking was done in AC buffer with 2% milk and 1 mM Dithiothreitol for at least one hour. Five microgram per milliliter of each of the recombinant proteins probes (GST, GST-Ndel1, GST-Pep3, GST-DID and GST-Nde1) were incubated with the membranes overnight at 4℃ rotating. Afterwards, the membranes were washed 3 times for 20 minutes in AC buffer and incubated with mouse anti-GST antibodies (UC Davis/NINDS/NIMH NeuroMab Facility). Following incubation with HRP-anti-mouse secondary antibodies the blots were developed with ECL and exposed to films. The membranes were then stained with Ponceau S to visualize the bait proteins.

Acknowledgements

We thank current and previous lab members for their contribution, Dr Elaine Bearer for her generous introduction to the squid system and usage of her instruments, Derek Nobrega for showing us the squid axon related experimental procedure, Joe DeGiorgis, Captain Henry Klimm, Captain Bill Klimm, Ed Enos and Louis Kerr for help in Woods Hole. O.R. is an Incumbent of the Berstein-Mason professorial chair of Neurochemistry.

M.E. is supported by the Gerhardt M. J. Schmidt Minerva Center for Supramolecular Architecture, and by the historic generosity of the Harold Perlman Family. Our research (O.R. and M.S.) has been supported in part by the Gruss Lipper Family Foundation Fellowship, the Israel Science Foundation (grant no. 270/04), the Legacy Heritage Biomedical Program of the Israel Science Foundation (grant no. 1062/08), BSF grant 2007081, Minerva foundation with funding from the Federal German Ministry for Education and Research, ERANET-NEURON (DISCover, IMOS 3-00000-6785), the Benoziyo Center for Neurological diseases, the Helen and Martin Kimmel Stem Cell Research Institute, and the David and Fela Shapell Family Center for Genetic Disorders Research.

References

Allen, R. D., Metuzals, J., Tasaki, I., Brady, S. T. and Gilbert, S. P. (1982). Fast axonal transport in squid giant axon. *Science* **218**, 1127-1129.

Ally, S., Larson, A. G., Barlan, K., Rice, S. E. and Gelfand, V. I. (2009). Opposite-polarity motors activate one another to trigger cargo transport in live cells. *J. Cell Biol.* **187**, 1071-1082.

Bearer, E. L. and Reese, T. S. (1999). Association of actin filaments with axonal microtubule tracts. *J. Neurocytol.* **28**, 85-98.

Bearer, E. L., Breakefield, X. O., Schuback, D., Reese, T. S. and LaVail, J. H. (2000). Retrograde axonal transport of herpes simplex virus: evidence for a single mechanism and a role for tegument. *Proc. Natl. Acad. Sci. USA* **97**, 8146-8150.

Berezuk, M. A. and Schroer, T. A. (2007). Dynactin enhances the processivity of kinesin-2. *Traffic* **8**, 124-129.

Blangy, A., Arnaud, L. and Nigg, E. A. (1997). Phosphorylation by p34cdc2 protein kinase regulates binding of the kinesin-related motor HsEg5 to the dynactin subunit p150. *J. Biol. Chem.* **272**, 19,418-19,424.

Bradshaw, N. J., Christie, S., Soares, D. C., Carlyle, B. C., Porteous, D. J. and Millar, J. K. (2009). NDE1 and NDEL1: multimerisation, alternate splicing and DISC1 interaction. *Neurosci. Lett.* **449**, 228-233.

Brady, S. T., Lasek, R. J. and Allen, R. D. (1982). Fast axonal transport in extruded axoplasm from squid giant axon. *Science* **218**, 1129-1131.

Brady, S. T., Lasek, R. J. and Allen, R. D. (1985). Video microscopy of fast axonal transport in extruded axoplasm: a new model for study of molecular mechanisms. *Cell Motil.* **5**, 81-101.

Chevalier-Larsen, E. and Holzbaur, E. L. (2006). Axonal transport and neurodegenerative disease. *Biochim. Biophys. Acta* **1762**, 1094-1108.

Colin, E., Zala, D., Liot, G., Rangone, H., Borrell-Pages, M., Li, X. J., Saudou, F. and Humbert, S. (2008). Huntingtin phosphorylation acts as a molecular switch for anterograde/retrograde transport in neurons. *EMBO J.* **27**, 2124-2134.

Coy, D. L., Hancock, W. O., Wagenbach, M. and Howard, J. (1999). Kinesin's tail domain is an inhibitory regulator of the motor domain. *Nat. Cell Biol.* **1**, 288-292.

Deacon, S. W., Serpinskaya, A. S., Vaughan, P. S., Lopez Fanarraga, M., Vernos, I., Vaughan, K. T. and Gelfand, V. I. (2003). Dynactin is required for bidirectional organelle transport. *J. Cell Biol.* **160**, 297-301.

DeGiorgis, J. A., Petukhova, T. A., Evans, T. A. and Reese, T. S. (2008). Kinesin-3 is an organelle motor in the squid giant axon. *Traffic* **9**, 1867-1877.

Degiorgis, J. A., Cavaliere, K. R. and Burbach, J. P. (2011). Identification of molecular motors in the Woods Hole squid, Loligo pealei: an expressed sequence tag approach. *Cytoskeleton* **68**, 566-577.

Derewenda, U., Tarricone, C., Choi, W. C., Cooper, D. R., Lukasik, S., Perrina, F., Tripathy, A., Kim, M. H., Cafiso, D. S., Musacchio, A. et al. (2007). The structure of the coiled-coil domain of Ndel1 and the basis of its interaction with Lis1, the causal protein of Miller-Dieker lissencephaly. *Structure* **15**, 1467-1481.

Dixit, R., Ross, J. L., Goldman, Y. E. and Holzbaur, E. L. (2008). Differential regulation of dynein and kinesin motor proteins by tau. *Science* **319**, 1086-1089.

Dompierre, J. P., Godin, J. D., Charrin, B. C., Cordelieres, F. P., King, S. J., Humbert, S. and Saudou, F. (2007). Histone deacetylase 6 inhibition compensates for the transport deficit in Huntington's disease by increasing tubulin acetylation. *J. Neurosci.* **27**, 3571-3583.

Duncan, J. E. and Goldstein, L. S. (2006). The genetics of axonal transport and axonal transport disorders. *PLoS Genet.* **2**, e124.

Encalada, S. E., Szpankowski, L., Xia, C. and Goldstein, L. S. (2011). Stable kinesin and dynein assemblies drive the axonal transport of mammalian prion protein vesicles. *Cell* **144**, 551-565.

Erck, C., Peris, L., Andrieux, A., Meissirel, C., Gruber, A. D., Vernet, M., Schweitzer, A., Saoudi, Y., Pointu, H., Bosc, C. et al. (2005). A vital role of tubulin-tyrosine-ligase for neuronal organization. *Proc. Natl. Acad. Sci. USA* **102**, 7853-7858.

Feng, Y. and Walsh, C. A. (2004). Mitotic spindle regulation by Nde1 controls cerebral cortical size. *Neuron* **44**, 279-293.

Feng, Y., Olson, E. C., Stukenberg, P. T., Flanagan, L. A., Kirschner, M. W. and Walsh, C. A. (2000). LIS1 regulates CNS lamination by interacting with mNudE, a central component of the centrosome. *Neuron* **28**, 665-679.

Gross, S. P. (2003). Dynactin: coordinating motors with opposite inclinations. *Curr. Biol.* **13**, R320-R322.

Gross, S. P. (2004). Hither and yon: a review of bi-directional microtubule-based transport. *Phys. Biol.* **1**, R1-R11.

Gross, S. P., Welte, M. A., Block, S. M. and Wieschaus, E. F. (2002). Coordination of opposite-polarity microtubule motors. *J. Cell Biol.* **156**, 715-724.

Guerin, T., Prost, J., Martin, P. and Joanny, J. F. (2010). Coordination and collective properties of molecular motors: theory. *Curr. Opin. Cell Biol.* **22**, 14-20.

Haghnia, M., Cavalli, V., Shah, S. B., Schimmelpfeng, K., Brusch, R., Yang, G., Herrera, C., Pilling, A. and Goldstein, L. S. (2007). Dynactin is required for coordinated bidirectional motility, but not for dynein membrane attachment. *Mol. Biol. Cell* **18**, 2081-2089.

Hendricks, A. G., Perlson, E., Ross, J. L., Schroeder, H. W., 3rd, Tokito, M. and Holzbaur, E. L. (2010). Motor coordination via a tug-of-war mechanism drives bidirectional vesicle transport. *Curr. Biol.* **20**, 697-702.

Hirohashi, Y., Wang, Q., Liu, Q., Du, X., Zhang, H., Sato, N. and Greene, M. I. (2006a). p78/MCRS1 forms a complex with centrosomal protein Nde1 and is essential for cell viability. *Oncogene* **25**, 4937-4946.

Hirohashi, Y., Wang, Q., Liu, Q., Li, B., Du, X., Zhang, H., Furuuchi, K., Masuda, K., Sato, N. and Greene, M. I. (2006b). Centrosomal proteins Nde1 and Su48 form a complex regulated by phosphorylation. *Oncogene* **25**, 6048-6055.

Holzbaur, E. L. (2004). Motor neurons rely on motor proteins. *Trends Cell Biol.* **14**, 233-240.

Holzbaur, E. L. and Goldman, Y. E. (2010). Coordination of molecular motors: from in vitro assays to intracellular dynamics. *Curr. Opin. Cell Biol.* **22**, 4-13.

Howard, J., Hudspeth, A. J. and Vale, R. D. (1989). Movement of microtubules by single kinesin molecules. *Nature* **342**, 154-158.

Ikegami, K., Heier, R. L., Taruishi, M., Takagi, H., Mukai, M., Shimma, S., Taira, S., Hatanaka, K., Morone, N., Yao, I. et al. (2007). Loss of alpha-tubulin polyglutamylation in ROSA22 mice is associated with abnormal targeting of KIF1A and modulated synaptic function. *Proc. Natl. Acad. Sci. USA* **104**, 3213-3218.

Kardon, J. R. and Vale, R. D. (2009). Regulators of the cytoplasmic dynein motor. *Nat. Rev. Mol. Cell Biol.* **10**, 854-865.

King, S. J. and Schroer, T. A. (2000). Dynactin increases the processivity of the cytoplasmic dynein motor. *Nat. Cell Biol.* **2**, 20-24.

King, S. J., Bonilla, M., Rodgers, M. E. and Schroer, T. A. (2002). Subunit organization in cytoplasmic dynein subcomplexes. *Protein Sci.* **11**, 1239-1250.

Kuznetsov, S. A., Langford, G. M. and Weiss, D. G. (1992). Actin-dependent organelle movement in squid axoplasm. *Nature* **356**, 722-755.

Levy, J. R. and Holzbaur, E. L. (2006). Cytoplasmic dynein/dynactin function and dysfunction in motor neurons. *Int. J. Dev. Neurosci.* **24**, 103-111.

Liang, Y., Yu, W., Li, Y., Yang, Z., Yan, X., Huang, Q. and Zhu, X. (2004). Nudel functions in membrane traffic mainly through association with Lis1 and cytoplasmic dynein. *J. Cell Biol.* **164**, 557-566.

Ligon, L. A., Tokito, M., Finklestein, J. M., Grossman, F. E. and Holzbaur, E. L. (2004). A direct interaction between cytoplasmic dynein and kinesin I may coordinate motor activity. *J. Biol. Chem.* **279**, 19,201-19,208.

Ma, S. and Chisholm, R. L. (2002). Cytoplasmic dynein-associated structures move bidirectionally in vivo. *J. Cell Sci.* **115**, 1453-1460.

Mandelkow, E. M., Thies, E., Trinczek, B., Biernat, J. and Mandelkow, E. (2004). MARK/PAR1 kinase is a regulator of microtubule-dependent transport in axons. *J. Cell Biol.* **167**, 99-110.

Martin, B. R. and Cravatt, B. F. (2009). Large-scale profiling of protein palmitoylation in mammalian cells. *Nat. Methods* **6**, 135-138.

Martin, M., Iyadurai, S. J., Gassman, A., Gindhart, J. G., Jr, Hays, T. S. and Saxton, W. M. (1999). Cytoplasmic dynein, the dynactin complex, and kinesin are interdependent and essential for fast axonal transport. *Mol. Biol. Cell* **10**, 3717-3728.

McKenney, R. J., Vershinin, M., Kunwar, A., Vallee, R. B. and Gross, S. P. (2010). LIS1 and NudE induce a persistent dynein force-producing state. *Cell* **141**, 304-314.

Mesngon, M. T., Tarricone, C., Hebbar, S., Guillotte, A. M., Schmitt, E. W., Lanier, L., Musacchio, A., King, S. J. and Smith, D. S. (2006). Regulation of cytoplasmic dynein ATPase by Lis1. *J. Neurosci.* **26**, 2132-2139.

Muller, M. J., Klumpp, S. and Lipowsky, R. (2008). Tug-of-war as a cooperative mechanism for bidirectional cargo transport by molecular motors. *Proc. Natl. Acad. Sci. USA* **105**, 4609-4614.

Muller, M. J., Klumpp, S. and Lipowsky, R. (2010). Bidirectional transport by molecular motors: enhanced processivity and response to external forces. *Biophys. J.* **98**, 2610-2618.

Myers, K. R., Lo, K. W., Lye, R. J., Kogoy, J. M., Soura, V., Hafezparast, M. and Pfister, K. K. (2007). Intermediate chain subunit as a probe for cytoplasmic dynein function: biochemical analyses and live cell imaging in PC12 cells. *J. Neurosci. Res.* **85**, 2640-2647.

Niethammer, M., Smith, D. S., Ayala, R., Peng, J., Ko, J., Lee, M. S., Morabito, M. and Tsai, L. H. (2000). NUDEL is a novel Cdk5 substrate that associates with LIS1 and cytoplasmic dynein. *Neuron* **28**, 697-711.

Peris, L., Thery, M., Faure, J., Saoudi, Y., Lafanechere, L., Chilton, J. K., Gordon-Weeks, P., Galjart, N., Bornens, M., Wordeman, L. et al. (2006). Tubulin tyrosination is a major factor affecting the recruitment of CAP-Gly proteins at microtubule plus ends. *J. Cell Biol.* **174**, 839-849.

Perlson, E., Jeong, G. B., Ross, J. L., Dixit, R., Wallace, K. E., Kalb, R. G. and Holzbaur, E. L. (2009). A switch in retrograde signaling from survival to stress in rapid-onset neurodegeneration. *J. Neurosci.* **29**, 9903-9917.

Prilusky, J., Felder, C. E., Zeev-Ben-Mordehai, T., Rydberg, E. H., Man, O., Beckmann, J. S., Silman, I. and Sussman, J. L. (2005). FoldIndex: a simple tool to predict whether a given protein sequence is intrinsically unfolded. *Bioinformatics* **21**, 3435-3438.

Reed, N. A., Cai, D., Blasius, T. L., Jih, G. T., Meyhofer, E., Gaertig, J. and Verhey, K. J. (2006). Microtubule acetylation promotes kinesin-1 binding and transport. *Curr. Biol.* **16**, 2166-2172.

Rogers, S. L., Tint, I. S., Fanapour, P. C. and Gelfand, V. I. (1997). Regulated bidirectional motility of melanophore pigment granules along microtubules in vitro. *Proc. Natl. Acad. Sci. USA* **94**, 3720-3725.

Sasaki, S., Shionoya, A., Ishida, M., Gambello, M. J., Yingling, J., Wynshaw-Boris, A. and Hirotsune, S. (2000). A LIS1/NUDEL/cytoplasmic dynein heavy chain complex in the developing and adult nervous system. *Neuron* **28**, 681-696.

Satpute-Krishnan, P., DeGiorgis, J. A. and Bearer, E. L. (2003). Fast anterograde transport of herpes simplex virus: role for the amyloid precursor protein of Alzheimer's disease. *Aging Cell* **2**, 305-318.

Satpute-Krishnan, P., DeGiorgis, J. A., Conley, M. P., Jang, M. and Bearer, E. L. (2006). A peptide zipcode sufficient for anterograde transport within amyloid precursor protein. *Proc. Natl. Acad. Sci. USA* **103**, 16532-16537.

Schnapp, B. J. and Reese, T. S. (1989). Dynein is the motor for retrograde axonal transport of organelles. *Proc. Natl. Acad. Sci. USA* **86**, 1548-1552.

Schroer, T. A. (2004). Dynactin. *Annu. Rev. Cell Dev. Biol.* **20**, 759-779.

Scott, D. A., Das, U., Tang, Y. and Roy, S. (2011). Mechanistic logic underlying the axonal transport of cytosolic proteins. *Neuron* **70**, 441-454.

Seitz, A., Kojima, H., Oiwa, K., Mandelkow, E. M., Song, Y. H. and Mandelkow, E. (2002). Single-molecule investigation of the interference between kinesin, tau and MAP2c. *EMBO J.* **21**, 4896-4905.

Shim, S. Y., Samuels, B. A., Wang, J., Neumayer, G., Belzil, C., Ayala, R., Shi, Y., Shi, Y., Tsai, L. H. and Nguyen, M. D. (2008). Ndel1 controls the dynein-mediated transport of vimentin during neurite outgrowth. *J. Biol. Chem.* **283**, 12,232-12,240.

Shmueli, A., Segal, M., Sapir, T., Tsutsumi, R., Noritake, J., Bar, A., Sapoznik, S., Fukata, Y., Orr, I., Fukata, M. et al. (2010). Ndel1 palmitoylation: a new mean to regulate cytoplasmic dynein activity. *EMBO J.* **29**, 107-119.

Shubeita, G. T., Tran, S. L., Xu, J., Vershinin, M., Cermelli, S., Cotton, S. L., Welte, M. A. and Gross, S. P. (2008). Consequences of motor copy number on the intracellular transport of kinesin-1-driven lipid droplets. *Cell* **135**, 1098-1107.

Song, Y., Benison, G., Nyarko, A., Hays, T. S. and Barbar, E. (2007). Potential role for phosphorylation in differential regulation of the assembly of dynein light chains. *J. Biol. Chem.* **282**, 17,272-17,279.

Stehman, S. A., Chen, Y., McKenney, R. J. and Vallee, R. B. (2007). NudE and NudEL are required for mitotic progression and are involved in dynein recruitment to kinetochores. *J. Cell Biol.* **178**, 583-594.

Stokin, G. B. and Goldstein, L. S. (2006). Axonal transport and Alzheimer's disease. *Annu. Rev. Biochem.* **75**, 607-627.

Terada, S., Kinjo, M. and Hirokawa, N. (2000). Oligomeric tubulin in large transporting complex is transported via kinesin in squid giant axons. *Cell* **103**, 141-155.

Terasaki, M., Schmidek, A., Galbraith, J. A., Gallant, P. E. and Reese, T. S. (1995). Transport of cytoskeletal elements in the squid giant axon. *Proc. Natl. Acad. Sci. USA* **92**, 11,500-11,503.

Toba, S., Watanabe, T. M., Yamaguchi-Okimoto, L., Toyoshima, Y. Y. and Higuchi, H. (2006). Overlapping hand-over-hand mechanism of single molecular motility of cytoplasmic dynein. *Proc. Natl. Acad. Sci. USA* **103**, 5741-5745.

Vale, R. D., Reese, T. S. and Sheetz, M. P. (1985a). Identification of a novel force-generating protein, kinesin, involved in microtubule-based motility. *Cell* **42**, 39-50.

Vale, R. D., Schnapp, B. J., Mitchison, T., Steuer, E., Reese, T. S. and Sheetz, M. P. (1985b). Different axoplasmic proteins generate movement in opposite directions along microtubules in vitro. *Cell* **43**, 623-632.

Vale, R. D., Schnapp, B. J., Reese, T. S. and Sheetz, M. P. (1985c). Organelle, bead, and microtubule translocations promoted by soluble factors from the squid giant axon. *Cell* **40**, 559-569.

Vale, R. D., Funatsu, T., Pierce, D. W., Romberg, L., Harada, Y. and Yanagida, T. (1996). Direct observation of single kinesin molecules moving along microtubules. *Nature* **380**, 451-453.

Vallee, R. B., Williams, J. C., Varma, D. and Barnhart, L. E. (2004). Dynein: an ancient motor protein involved in multiple modes of transport. *J. Neurobiol.* **58**, 189-200.

Vaughan, P. S., Leszyk, J. D. and Vaughan, K. T. (2001). Cytoplasmic dynein intermediate chain phosphorylation regulates binding to dynactin. *J. Biol. Chem.* **276**, 26,171-26,179.

Vermot, J., Fraser, S. E. and Liebling, M. (2008). Fast fluorescence microscopy for imaging the dynamics of embryonic development. *HFSP J.* **2**, 143-155.

Vershinin, M., Carter, B. C., Razafsky, D. S., King, S. J. and Gross, S. P. (2007). Multiple-motor based transport and its regulation by Tau. *Proc. Natl. Acad. Sci. USA* **104**, 87-92.

Vershinin, M., Xu, J., Razafsky, D. S., King, S. J. and Gross, S. P. (2008). Tuning microtubule-based transport through filamentous MAPs: the problem of dynein. *Traffic* **9**, 882-892.

Wang, S. and Zheng, Y. (2010). Identification of a novel dynein-binding domain in Nudel essential for spindle pole organization in Xenopus egg extracts. *J. Biol. Chem.* **286**, 587-593.

Yamada, M., Toba, S., Yoshida, Y., Haratani, K., Mori, D., Yano, Y., Mimori-Kiyosue, Y., Nakamura, T., Itoh, K., Fushiki, S. et al. (2008). LIS1 and NDEL1 coordinate the plus-end-directed transport of cytoplasmic dynein. *EMBO J.* **27**, 2471-2483.

Yan, X., Li, F., Liang, Y., Shen, Y., Zhao, X., Huang, Q. and Zhu, X. (2003). Human Nudel and NudE as regulators of cytoplasmic dynein in poleward protein transport along the mitotic spindle. *Mol. Cell. Biol.* **23**, 1239-1250.

Zhang, Q., Wang, F., Cao, J., Shen, Y., Huang, Q., Bao, L. and Zhu, X. (2009). Nudel promotes axonal lysosome clearance and endo-lysosome formation via dynein-mediated transport. *Traffic* **10**, 1337-1349.

Zylkiewicz, E., Kijanska, M., Choi, W. C., Derewenda, U., Derewenda, Z. S. and Stukenberg, P. T. (2011). The N-terminal coiled-coil of Ndel1 is a regulated scaffold that recruits LIS1 to dynein. *J. Cell Biol.* **192**, 433-445.